Electrochemical Properties of Nanocrystalline La$_{0.5}$Sr$_{0.5}$CoO$_{3-x}$ Thin Films[†]

Shuangyan Wang,[‡] Jongsik Yoon,[§] Guntae Kim,[‡] Daxiang Huang,[‡] Haiyan Wang,[§] and Allan J. Jacobson*,[‡]

[‡]*Department of Chemistry, University of Houston, Houston, Texas 77204-5003, and* [§]*Department of Electrical Engineering, Texas A&M University, College Station, Texas 77843-3128*

As part of an investigation of new cathode materials for intermediate temperature solid oxide fuel cells, we have investigated several perovskite oxides with cobalt ions on the B sites in both bulk and thin film forms. Of particular interest is the composition La$_{0.5}$Sr$_{0.5}$CoO$_{3-x}$ (LSCO) which has exceptional properties for oxygen reduction at intermediate temperatures in ceria based fuel cells. Thin films of LSCO were deposited on both sides of a dense polycrystalline gadolinia doped ceria substrate by pulsed laser deposition under conditions that lead to the formation of nanocrystalline films. The electrochemical properties for oxygen reduction were determined in a symmetric electrochemical cell by alternating current (AC) impedance spectroscopy. The results were analyzed using the Adler−Lane−Steele (ALS) model to obtain the diffusion and surface exchange coefficients and the thermodynamic factor. We show that the thermodynamic factor, a measure of how easy it is to create oxygen vacancies, is much higher than observed in conventional cathodes. As a result, the electrode composition changes little with temperature and oxygen partial pressure, the large chemical contribution to the thermal expansion is reduced, and the electrode has good stability. The use of a nanostructured electrode does not significantly affect the fundamental material parameters (surface exchange and diffusion coefficients), and the very low area specific resistance (0.09 ohm cm^2 at 600 °C) observed is because the synthesis method gives a very high surface area (80 μm^{-1}).

Introduction

Mixed ionic−electronic conductors can be used as electrodes[1] in solid oxide fuel cells (SOFCs), sensors,[2] and oxygen-separation ion-transport membranes.[3] SOFCs have the promise to improve energy efficiency and to provide society with a clean energy-producing technology. Critical goals for widespread commercialization of solid oxide fuel cells are to lower cost and to enhance stability by reducing the operating temperature to 500−700 °C.[4] Micro-solid-oxide fuel cells (μ-SOFCs) with a total thickness in the micrometer range are predicted to have 3−4 times higher energy densities than Li-ion batteries but also require lowering the operating temperature to at least 550 °C.[5] Consequently, many recent studies

have focused on lower operating temperatures,[6−12] where the primary factor that limits power output is the slow rate of oxygen reduction that leads to significant cathodic polarization.

Strontium-doped LaCoO$_3$ (LSCO) electrodes have fast oxygen transport kinetics and high electronic conductivity and have been studied previously with ceria electrolytes; LSCO does not react with gadolinia doped ceria (CGO) to form insulating phases, and CGO has sufficiently high oxygen ion conductivity and low electronic conductivity for use at intermediate temperatures.[13,14]

AC impedance is one commonly used method to evaluate the cathode performance and has been used in previous studies of LSCO cathodes either of dense films or porous films with small surface area. Yang et al.[15] studied 0.25 and 0.5 μm dense thick films of La$_{0.5}$Sr$_{0.5}$CoO$_{3-x}$ on YSZ single crystal substrates in various

[†] Accepted as part of the 2010 "Materials Chemistry of Energy Conversion Special Issue".
*Corresponding author. E-mail: ajjacob@uh.edu. Tel.: 713-743-2785. Fax: 713-743-2787.
(1) Adler, S. B. *Chem. Rev.* **2004**, *104*, 4791.
(2) Tunney, J. J.; Post, M. L. *J. Electroceram.* **2000**, *5*, 63.
(3) Bouwmeester, H. J. M.; Burggraaf, A. J. *The CRC Handbook of Solid State Electrochemistry*; CRC Press: Boca Raton, 1997.
(4) Ralph, J. M.; Rossignol, C; Kumar, R. *J. Electrochem. Soc.* **2003**, *150*, A1518.
(5) Bieberle-Hutter, A.; Beckel, D.; Muecke, U. P.; Rupp, J. L. M.; Infortuna, A; Gauckler, L. J. *MST News* **2005**, *4/05*, 12.
(6) Kilner, J. A.; Shaw, C. K. M. *Solid State Ionics* **2002**, *154−155*, 523.
(7) Read, M. S. D.; Islam, M. S.; Watson, G. W.; Hancock, F. E. *J. Mater. Chem.* **2001**, *11*, 2597.
(8) Bassat, J. M.; Odier, P.; Villesuzanne, A.; Marin, C.; Pouchard, M. *Solid State Ionics* **2004**, *167*, 341.

(9) Skinner, S. J; Kilner, J. A. *Solid State Ionics* **2000**, *135*, 709.
(10) Kim, G.; Wang, S.; Jacobson, A. J.; Reimus, L.; Brodersen, P.; Mims, C. A. *J. Mater. Chem.* **2007**, *17*, 2500.
(11) Kim, G.; Wang, S.; Jacobson, A. J.; Yuan, Z.; Donner, W.; Chen, C. L.; Reimus, L.; Brodersen, P.; Mims, C. A. *Appl. Phys. Lett.* **2006**, *88*, 024103.
(12) Taskin, A. A.; Lavrov, A. N.; Ando, Y. *Appl. Phys. Lett.* **2005**, *86*, 091910.
(13) Ralph, J. M.; Schoeler, A. C.; Krumpelt, M. *J. Mater. Sci.* **2001**, *36*, 1161.
(14) Doshi, R.; Richards, V. L.; Carter, J. D.; Wang, X.; Krumpelt, M. *J. Electrochem. Soc.* **1999**, *146*, 1273.
(15) Yang, Y. L.; Chen, C. L.; Chen, S. Y.; Chu, C. W.; Jacobson, A. J. *J. Electrochem. Soc.* **2000**, *147*, 4001.

oxygen pressures between 500 and 750 °C and concluded that the electrode reaction was limited by the surface exchange reaction. Kawada investigated a dense 1.5-μm-thick polycrystalline film of $La_{0.6}Sr_{0.4}CoO_{3-x}$ on a CGO substrate in 10^{-4}–1 atm O_2 at 600–800 °C where the surface process was also considered to be the rate-determining step.[16] Bieberle-Hütter et al.[17] made dense thin films (100–150 nm) of $La_{0.5}Sr_{0.5}CoO_{3-x}$ with interdigitated electrode patterns on CGO–SiO_2 and measured their AC impedance spectra in air from 276 to 403 °C. Adler[18] studied porous electrodes of $La_{1-x}Sr_xCoO_3$ (x = 0.2, 0.3, and 0.4) with surface areas $\sim$2 μm^{-1} between 550 and 800 °C and analyzed the data using the Adler–Lane–Steele (ALS) model[19] to obtain the surface exchange coefficient and the oxygen vacancy diffusion coefficient.

Cathodes containing nanoparticles prepared by infiltration of porous electrodes with high surface area and improved performance have been reported.[20–23] For example, Zhao et al. made 50-μm thick films consisting of 50-nm particles of $La_{0.6}Sr_{0.4}CoO_{3-x}$ embedded in a CGO cathode frame and obtained area specific resistance (ASR) values of 0.281–0.306 Ω cm^2 at 600 °C which were stable for 3 months. Cathodes formed directly from nanoparticles were described by Peters et al.[24] Nanoporous LSCO cathodes with film thicknesses in the range 200–300 nm and grain sizes of 50 nm were prepared by metal organic deposition (MOD) on YSZ with and without a 5 μm CGO interlayer. With a CGO interlayer, stable behavior and very low polarization resistances were observed in the temperature range 500–700 °C.

The transport properties of mixed conducting nanoparticles cannot be studied easily by commonly used methods, such as electrical conductivity relaxation, weight relaxation, and secondary ion mass spectroscopy methods which require dense samples generally made at high temperatures where the nanoparticles sinter. Consequently, in this work, we have used AC impedance to study porous nanocrystalline LSCO thin films with very high surface area deposited by pulsed laser deposition on a dense polycrystalline CGO substrate. The film preparation and some preliminary electrochemical studies were reported previously.[25] The results obtained in this study were analyzed in terms of fundamental materials parameters namely the oxygen ion diffusion coefficient, the oxygen surface exchange rate, and the thermodynamic

factor using the ALS model, at temperatures low enough to keep the nanoporous structure intact. We show that the thermodynamic factor, a measure of how easy it is to create oxygen vacancies, is much higher than observed in conventional cathodes. As a result, the electrode composition changes little with temperature and oxygen partial pressure, the large chemical contribution to the thermal expansion is reduced, and the electrode has good stability. The use of a nanostructured electrode does not significantly affect the fundamental material parameters (surface exchange and diffusion coefficients), and the very low area specific resistance observed (0.09 ohm cm^2 at 600 °C) is because the synthesis method gives a very high surface area (80 μm^{-1}).

Experimental Section

Synthesis. Deposition of the LSCO cathode layers was performed in a 12 in. vacuum chamber with a KrF excimer laser (Lambda Physik 210, λ = 248 nm, 10 Hz) on a CGO substrate at a typical background pressure of 1×10^{-6} mbar. The laser beam was focused to obtain an energy density of approximately 5 J cm^{-2} at a 45° angle of incidence. The hot-pressed LSCO target and CGO electrolyte disks were all prepared by mixing stoichiometric amounts of powders namely La_2O_3, $Sr(NO_3)_2$, Co_3O_4, CeO_2, and Gd_2O_3 followed by high temperature sintering. The LSCO thin film cathode layers were deposited in one step under the same conditions as reported in our previous work using the pulsed laser deposition technique.[25] The growth rate for the thin film was controlled at about 1 nm/s at an oxygen partial pressure of about 200 mTorr. The substrate temperature was kept at 300–500 °C to optimize the microstructure and the nanopore size of the cathode layer. The CGO disk is 1.05 cm in diameter and 1 mm in thickness. The LSCO film thickness (LSCO) on each side is $\sim$720 $\pm$ 20 nm estimated by scanning electron microscopy (SEM). The sample was single phase cubic perovskite by X-ray diffraction.

Microstructural Characterization. The surface morphology of the LSCO thin films determined by scanning electron microscopy was reported previously.[25] Here, a more detailed microstructural study based on high resolution transmission electron microscopy (TEM) and Z contrast imaging is presented. Cross-sectional TEM specimens were prepared through a conventional method including cutting, gluing, grinding, and polishing. Final thinning was performed using a Gatan Precision Ion Polishing System (PIPS). The substrate–film epitaxial relationships and interface structures were analyzed using a JEM 2010F field emission high-resolution TEM equipped with a Scanning Image Observation Device. Chemical compositions of microregions were measured using the energy-dispersive X-ray spectrometer (EDX) attached to the TEM.

Alternating Current (AC) Impedance Measurements. For AC impedance measurements, samples were spring-loaded into a homemade sample holder. Fine (100-mesh) gold gauzes were used as current collectors on both sides of the samples since Pt is known to catalyze the oxygen reduction reaction. AC impedance measurements were conducted with a Solatron Instruments 1260 impedance analyzer in the frequency range of 0.01 Hz to 1 MHz. A large electrical perturbation (amplitude: 80–100 mV) was used to increase the signal-to-noise ratio. Measurements were performed at $0.01 \le pO_2 \le 1$ atm and $350 \le T \le 600$ °C.

Theory. To obtain oxygen transport information from the AC impedance spectra, we adopted the ALS model.[18] This model is

(16) Kawada, T.; Suzuki, J.; Sase, M.; Kaimai, A.; Yashiro, K.; Nigara, Y.; Mizusaki, J.; Kawamura, K.; Yugami, H. *J. Electrochem. Soc.* **2002**, *149*, E252.
(17) Bieberle- Hütter, A.; Søgaard, M.; Tuller, H. L. *Solid State Ionics* **2006**, *177*, 1969.
(18) Adler, S. B. *Solid State Ionics* **1998**, *111*, 125.
(19) Adler, S. B.; Lane, J. A.; Steele, B. C. H. *J. Electrochem. Soc.* **1996**, *143*, 3554.
(20) Sholklapper, T. Z.; Jacobson, C. P.; Visco, S. J.; De Jonghe, L. C. *Fuel Cells* **2008**, *8*, 303.
(21) Sholklapper, T. Z.; Radmilovic, V.; Jacobson, C. P.; Visco, S. J.; De Jonghe, L. C. *Electrochem. Solid-State Lett.* **2007**, *10*, B74.
(22) Shah, M.; Barnett, S. A. *Solid State Ionics* **2008**, *179*, 2059.
(23) Zhao, F.; Peng, R.; Xia, C. *Mater. Res. Bul.* **2008**, *43*, 370.
(24) Peters, C.; Weber, A.; Ivers-Tiffee, E. *J. Electrochem. Soc.* **2008**, *155*, B730.
(25) Yoon, J.; Araujo, R.; Grunbaum, N.; Baque, L.; Serquis, A.; Caneiro, A.; Zhang, X.; Wang, H. *Appl. Surf. Sci.* **2007**, *254*, 266.
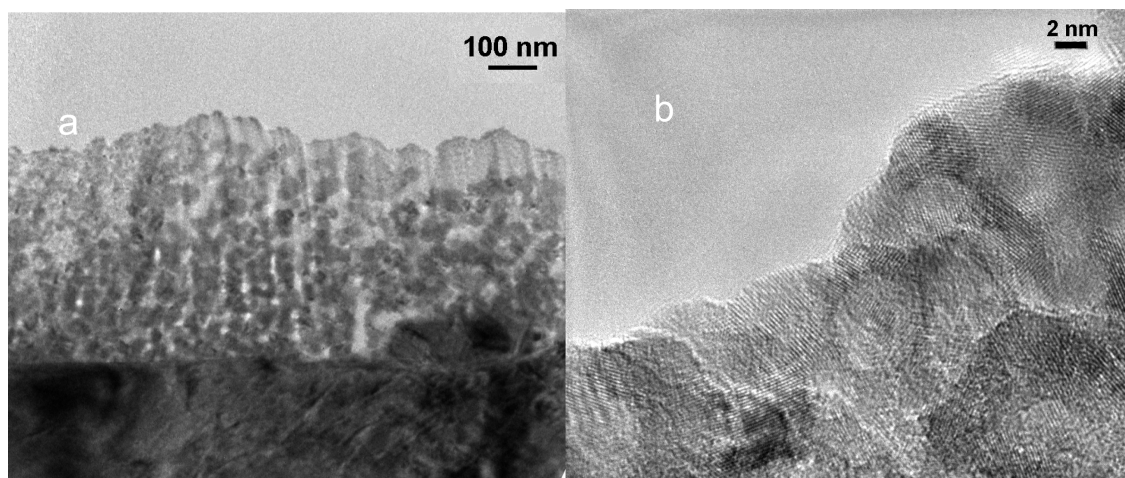
Figure 1. (a) Cross-sectional low magnification image for the entire film area and (b) HRTEM image around the film surface area of a LSCO/CGO film after the impedance measurements.

versatile in the sense that the mass transport is not limited to surface exchange reactions or bulk diffusion, and no specific reaction mechanism is required for the surface exchange reaction. The general equation for this model is

$$Z_{chem} = R_{chem}\sqrt{\frac{1}{1+j\omega t_{chem}}}\Big|\tanh\Big(\frac{L}{\delta}\sqrt{1+j\omega t_{chem}}\Big) \quad (1)$$

Where Z_{chem} is the impedance of the electrode reaction, R_{chem} is a characteristic resistance and t_{chem} is a characteristic time constant, L is the thickness of the electrode, and δ is a characteristic length that determines the transition from bulk to surface control of the reaction kinetics. According to the model, the following equations relate the macroscopic properties to the microscopic characteristics

$$R_{chem} = \Big(\frac{RT}{2F^2}\Big)\sqrt{\frac{\tau}{(1-\varepsilon)c_v D_v a r_0(\alpha_f + \alpha_b)}} \quad (2)$$

$$t_{chem} = \frac{c_v(1-\varepsilon)}{A_v a r_0(\alpha_f + \alpha_b)} \quad (3)$$

$$\delta = \sqrt{\frac{c_v D_v(1-\varepsilon)}{a r_0(\alpha_f + \alpha_b)\tau}} \quad (4)$$

where c_v is the oxygen vacancy concentration, D_v is the oxygen vacancy diffusion coefficient, ε is the porosity, a is the surface area, and τ is the tortuosity of the solid-phase of the porous electrode. A_v is the thermodynamic factor of oxygen vacancies defined as $A_v = (-1/2)\partial \ln pO_2/\partial \ln c_v$, r_0 is the exchange neutral flux density, and α_f and α_b are kinetic parameters with their sum as unity. The alphas are related to the self-surface exchange coefficient, k_i, and the lattice oxygen concentration, c_i, by $r_0(\alpha_f + \alpha_b) = k_i c_i$ where c_i can be approximated without introducing significant error by assuming that the oxygen stoichiometry is 3 (corresponding to ~0.091 mol cm^{-3}). Combining equations, we obtain

$$D_{chem} = \frac{\delta^2\tau}{t_{chem}} \quad \text{and} \quad D_i = \frac{RT\delta\tau}{2F^2 c_i(1-\varepsilon)}\frac{1}{R_{chem}} \quad (5)$$

$$k_{chem} = \frac{(1-\varepsilon)}{a t_{chem}} \quad \text{and} \quad k_i = \Big(\frac{RT}{2F^2}\Big)\frac{1}{\delta a R_{chem} c_i} \quad (6)$$

where D_{chem} and k_{chem} are the chemical diffusion and the chemical surface exchange coefficients, respectively. A_v can be expressed in term of the fitting parameters as

$$A_v = \frac{2F^2 c_v(1-\varepsilon)\delta R_{chem}}{RT t_{chem}} \quad (7)$$

Unfortunately, it is not possible to estimate the oxygen nonstoichiometry in the film to calculate c_v, and consequently, we use the thermodynamic factor for oxygen ions and the relationship $A_v c_i = A_i c_v$ to obtain

$$A_i = \frac{2F^2 c_i(1-\varepsilon)\delta R_{chem}}{RT t_{chem}} \quad (8)$$

A_i relates the self and chemical kinetic parameters by $A_i = D_{chem}/D_i = k_{chem}/k_i$. From the above relations and knowing the electrode microstructure, the transport parameters and thermodynamic factors can be obtained from the impedance spectra.
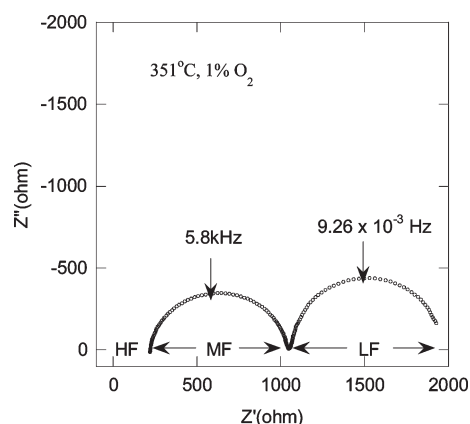
Results and Discussion

Microstructure. A low magnification cross-sectional TEM image covering both the LSCO film and the CGO substrate is shown in Figure 1a. The interface between the film and the substrate is very clear with no indication of interface reaction or intermixing. It shows a film with about 500−700 nm thickness on average which has a vertically aligned columnlike microstructure with a 25-nm-thick cap layer. Figure 1b is a higher resolution TEM image taken around the film surface cap layer, showing that the cap layer is actually made up of nanoparticles of LSCO with sizes ranging from 6 to 10 nm and about 8 nm on average. HRTEM imaging also confirms that the dark column film area as shown in Figure 1a has a much larger grain size of around 50 nm and that the grain size slightly increases from the top to bottom of the film. The light-contrast areas between the dark columns indicate porosity though some small-size nanoparticles of ~8 nm in diameter similar as those in the surface cap layer. The EDX measurements over the entire film area show the distribution of the chemical composition of the film. In the dark column area with a larger grain size, the ratio of
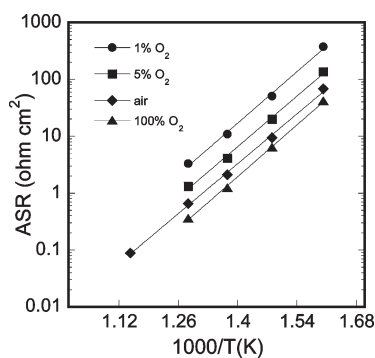
La:Sr:Co is ~1:1:2. The cap layer and the area between the dark columns have a similar chemical composition with a ratio of La:Sr:Co around 1:1:3 which is relatively Co-rich. The Z contrast imaging also confirms the similarity between the cap layer area and the area between the columns. The TEM observations indicate that the LSCO film is a nanocrystalline film with two types of different microstuctures. One is the dark column areas with a larger grain size of about 50 nm, and the other is porous with 8-nm-size nanoparticles in the cap layer and between the dark columns.

AC Impedance. Figure 2 shows a typical AC impedance spectrum of the LSCO/CGO/LSCO symmetrical cell. It has three distinct regions: high frequency (HF), medium frequency (MF), and low frequency (LF) regions. In all the spectra collected, oxygen partial pressures have little effect on the magnitude of both HF and MF regions. The capacitance of the MF region obtained by fitting to a depressed semicircle is ~10^{-8} F cm^{-2}, indicative of grain boundaries. Another CGO pellet (fabricated using the same method as the substrate) with Pt electrodes was then measured in air. A comparison of the spectra from the two samples showed that the HF and MF regions belonged to the grain and grain boundary, respectively, of the CGO substrate.

The resistance of the LF region decreases rapidly with increase of the oxygen partial pressure. The capacitance of the LF feature was estimated by fitting the data between ~0.03 and 0.2 Hz with a single RC circuit. The capacitance was found to be very large, in the range of $0.01-0.03$ F cm^{-2}, suggesting that it is a chemical capacitance. The magnitude of the chemical capacitance together with the strong oxygen pressure dependence indicates that the LF region originates from the electrode reaction.

The area specific resistance (ASR) of the cell is calculated from $R(\text{LF}) \times$ area/2 and is plotted in Figure 3. $R(\text{LF})$ is calculated by using the value of Z' at 0 Hz, which is estimated by extending the LF region into the real axis, minus the value of Z' at the onset of the LF region. The ASR decreases with increasing oxygen partial pressure and increasing temperature. The lowest ASR we obtained in air is 0.089 ohm cm^2 at 600 °C. A comparison of the results obtained here with literature results is given in Table 1. Zhao et al.[23] made La$_{0.6}$Sr$_{0.4}$CoO$_{3-x}$ electrodes impregnated into a porous Sm$_{0.2}$Ce$_{0.8}$O$_{1.9}$ (CSO) matrix

Figure 2. Typical AC impedance spectrum of the LSCO/CGO/LSCO symmetrical cell.

**Figure 3.** Electrode area specific resistance (ASR) calculated from the total electrode resistance.
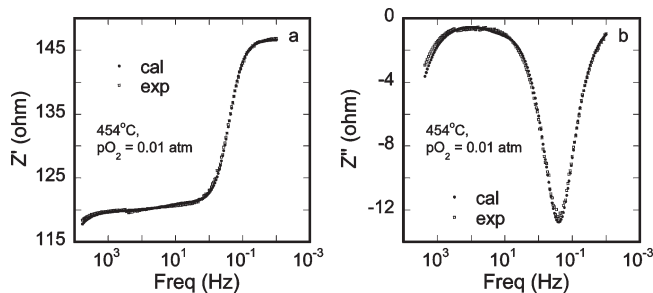
Figure 4. Representative example of the observed and calculated (a) real and (b) imaginary parts of the impedance spectra at 454 °C and pO$_2$ = 0.01 atm.

Table 1. Comparison of ASR Data for LSCO Cathodes

| cathode	La$_{0.5}$Sr$_{0.5}$CoO$_{3-x}$	La$_{0.6}$Sr$_{0.4}$CoO$_{3-x}$	La$_{0.5}$Sr$_{0.5}$CoO$_{3-x}$	La$_{0.5}$Sr$_{0.5}$CoO$_{3-x}$
fabrication method	PLD	ion impregnation	MOD	MOD
particle size	8 nm	~50 nm	54 ± 25 nm	54 ± 25
film thickness	720 ± 20 nm	~50 μm	300 nm	300 nm
electrolyte	CGO	CSO	YSZ	YSZ + 5 μm CGO
current collector	Au mesh	Pt paste	30 μm LSCF with Au mesh	30 μm LSCF with Au mesh
T (°C)			ASR Ω cm^2	
400[a]	11.29			
450[a]	2.57			
500[a]	0.71	2.5		
550[a]	0.23	0.7		
600	0.089	0.29	0.146	0.13
ref	this work	23	24	24

[a] Taken from plots of temperature dependence of ASR in Figure 3.
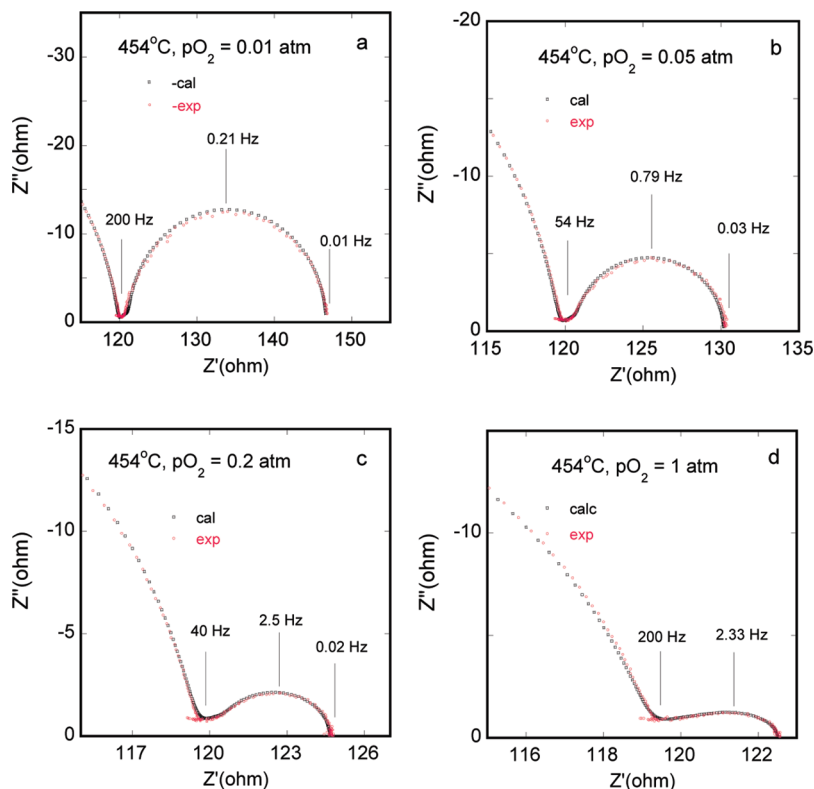
Figure 5. LF regions of the impedance spectra of the LSCO/CGO/LSCO symmetrical cell collected at different oxygen partial pressures. Circles are experimental data while squares are fitted data.

combined with a CSO electrolyte substrate. At 600 °C, ASR was only 0.29−0.31 ohm cm^2 for the impregnated electrode while it was 2.2−2.6 ohm cm^2 for a conventional electrode prepared using a conventional screen printing technique. The impregnated electrode also showed very good stability. Recently, Peters et al.[24] reported an ASR value of 0.13 Ω cm^2 at 592 °C in air for an electrode with nominal composition of $La_{0.5}Sr_{0.5}CoO_{3-x}$ prepared from nanosized particles. The ∼300-nm-thick LSCO electrode was made by spin coating of metal organic solutions. (La, Sr)(Co,Fe)O_{3-x} (LSCF) was used as a current collector.

In order to analyze the data, the following serial equivalent circuit was used to fit the impedance spectra. R_1 represents the resistance of bulk CGO (HF), R_2 represents the resistance of the grain boundaries of the CGO substrate (MF), in parallel with a CPE2 element to describe the depressed semicircle. Z_{chem} (eq 1) is the impedance of the LF feature. A program to fit the AC impedance data was written because Z_{chem} is typically not a built-in circuit element in instrument programs. Fitting parameters used were R_1, R_2, CPE$_2$-T, CPE$_2$-P, R_{chem}, t_{chem}, and L/δ.
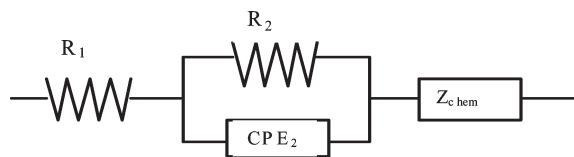
The experimental data and the fitting results for the cell at 454 °C in 0.01 atm O_2 are shown in Figure 4. The frequency dependence of Z' and Z'' is used to obtain a credible fit with seven fitting parameters in the model. The data at different oxygen partial pressures are shown as Cole−Cole plots in Figure 5. To emphasize the region corresponding to the electrode reaction, the HF regions and most of the MF regions are excluded from the plots. As we can see, the data are excellently described by this equivalent circuit.

The fitting results for Z_{chem} at all temperatures are listed in Table 2. The characteristic length decreases as the oxygen partial pressure and temperature increase, consistent with the shape of the LF region, which is close to a semicircle (more surface controlled) at 351 °C in 0.01 atm O_2 and becomes more like a a half pear (more diffusion like) at 506 °C in 0.2 atm O_2.

To obtain the kinetic parameters using the ALS model, the microstructure data listed in Table 3 were used. The surface area a of the film was estimated by modeling the film as composed of arrays of unconnected capped cylinders (see Figure 1). One capped cylinder is illustrated at the top of Table 3 with r as the radius of the cap and L as the thickness of the film. The tortuosity τ is estimated using the equation: $\tau = 1 - 0.49 \ln(1 - \varepsilon)$ with $(1 - \varepsilon)$ as the fraction of the phase that conducts oxygen ions.[26]

The chemical and self-diffusion coefficients derived from the analysis of the impedance data are shown in Figures 6 and 7. The self-diffusion coefficient shows little dependence on pO_2 at all temperatures. In general, $C_v D_v = C_i D_i$ with D_v being independent of pO_2. The lack of any
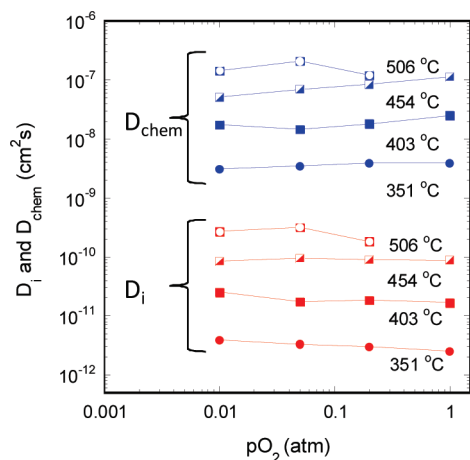
(26) Barrande, M.; Bouchet, R.; Denoyel, R. *Anal. Chem.* **2007**, *79*, 9115.

Table 2. Values of Parameters Used to Fit Z_{chem} of the LSCO/CGO/LSCO Symmetrical Cell Using the ALS Model

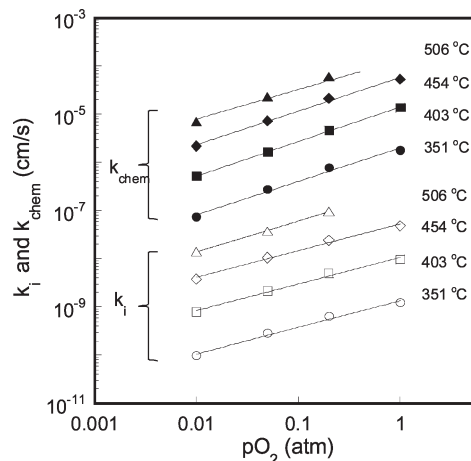| T (°C)	pO_2 (atm)	t_{chem} (s)	L/δ	R_{chem} (Ω)
351	0.01	19	0.30	267
	0.05	5.08	0.56	168
	0.2	1.80	0.88	119
	1	0.79	1.33	92.5
403	0.01	2.70	0.34	39.5
	0.05	0.84	0.67	29.0
	0.2	0.30	1	18.3
	1	0.10	1.47	13.8
454	0.01	0.63	0.41	10.5
	0.05	0.19	0.64	6.0
	0.2	0.065	1	4.05
	1	0.026	1.36	3.03
506	0.01	0.196	0.44	3.29
	0.05	0.060	0.66	1.86
	0.2	0.023	1.40	1.53

Table 3. Microstructure Data Used for Calculation of Kinetic Parameters of LSCO Film[a]

r	2.5×10^{-2}	μm
L	0.72	μm
a	81	μm^{-1}
ε	0.10	
τ	1.05	

[a] Surface area in squared meters per cubic meter or inverse meters.

Figure 6. Pressure dependence of the chemical and self-diffusion coefficients of $La_{0.5}Sr_{0.5}CoO_{3-x}$ in a LSCO/CGO/LSCO symmetrical cell.

pO_2 dependence for D_i implies that the oxygen vacancy concentration changes very little over this range of conditions.

If we lump the elementary steps of the surface oxygen reaction into the reaction: $^1/_2O_2 + V_O^{\cdot\cdot} \Leftrightarrow O_O^x + 2h\cdot$ with k_f and k_r as the overall forward and reverse reaction rate coefficients, then the self-surface exchange coefficient is written as $k_i = k_f(p/p_0)^{0.5}(c_v/c_i)$.[27] As indicated in Figure 6, the pressure dependence of the oxygen vacancy
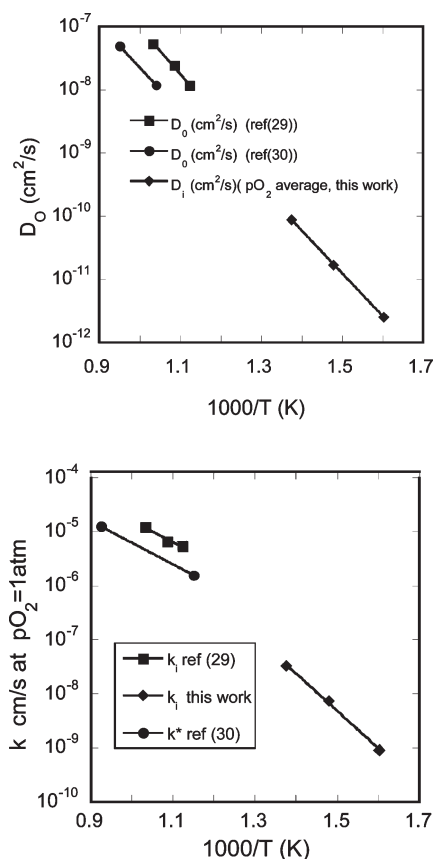
(27) Kim, S.; Wang, S.; Chen, X.; Yang, Y. L.; Wu, N.; Ignatiev, A.; Jacobson, A. J.; Abeles, B. *J. Electrochem. Soc.* **2000**, *147*, 2398.

Figure 7. Pressure dependence of the chemical and self-surface exchange coefficients of $La_{0.5}Sr_{0.5}CoO_{3-x}$ in a LSCO/CGO/LSCO symmetrical cell.
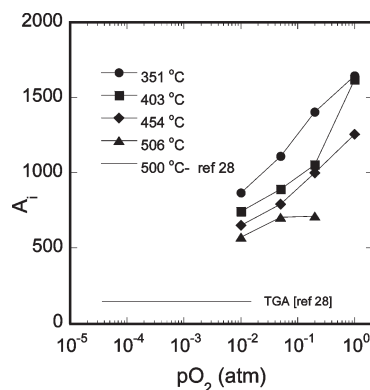
Figure 8. Thermodynamic factor as a function of pO_2 (atm) from 351 to 506 °C.

concentration is very small and consequently k_i would be expected to have a $pO_2^{1/2}$ dependence. The fits to the data, shown in Figure 7, are in reasonable agreement with this relation, with exponents close to 0.5 with the exception of the data at 506 °C where the value is somewhat larger ($\sim$0.6).

We were not able to fit the impedance spectrum at 600 °C in air, but by extrapolating the temperature dependence of k_i and D_i in air to 600 °C, we obtained 6.73×10^{-7} and 1.44×10^{-9} cm^2 s^{-1} for k_i and D_i, respectively. Using these two numbers and the ALS model, the calculated ASR of the LSCO film is 0.09 Ω cm^2, in agreement with the experimental value of 0.089 Ω cm^2. For the LSCO film reported by Peters et al.,[24] we estimated its ASR in air by using an average grain size of 54 nm, a thickness of 300 nm, and 20–60% porosity, the values of k_i and D_i above, and the ALS model. The value we obtain is between 0.115 and 0.145 Ω cm^2, in good agreement with their reported value of 0.13 Ω cm^2.

The thermodynamic factor, A_i of the electrode increases with increasing oxygen partial pressure and decreasing temperature as expected [Figure 8]. The large thermodynamic factor is consistent with the small change in c_v indicated by the pressure dependence of D_i and k_i. The magnitude and the oxygen pressure dependence of

Figure 9. Comparison of D_i and k_i with values reported in the literature.

the thermodynamic factor are much higher than that for the powder sample reported earlier[28] indicating that it is much more difficult to incorporate oxygen ions into the lattice of the film. Kawada made the same observation for a 1.5-μm thick dense film of $La_{0.6}Sr_{0.4}CoO_3$ on a polycrystalline CGO substrate and proposed that mechanical stress arising from the thermal expansion mismatches between the film and the substrate caused such an effect. Large thermodynamic factors may indicate smaller changes in composition and may give more stable performance by limiting thermal expansion.

Comparisons with Previous Studies. The present results for D_i and k_i are compared with literature data for bulk LSCO measured by electrical conductivity relaxation[29] and by isotope exchange and depth profiling[30] in Figure 9.

(28) Mizusaki, J.; Mima, Y.; Yamauchi, S.; Fueki, K.; Tagawa, H. *J. Solid State Chem.* **1989**, *80*, 102.
(29) Wang, S.; Verma, A.; Yang, Y. L.; Jacobson, A. J.; Abeles, B. *Solid State Ionics* **2001**, *140*, 125.
(30) De Souza, R. A.; Kilner, J. A. *Solid State Ionics* **1998**, *106*, 175.

Even though the temperature ranges of the measurements do not overlap, an extrapolation of the values of D_i measured in this work is in good agreement with the previous studies. In contrast, the k_i measured here has a higher activation energy but does extrapolate to about the same value as the higher temperature measurements.

Conclusions

LSCO electrodes with a porous nanostructure were made using the Pulsed Laser Deposition (PLD) method. AC impedance spectra were measured for a LSCO/CGO/LSCO symmetrical cell and were analyzed systematically using the ALS model. Provided that the microstructure of the electrode is known, then at least for the zero bias situation, the ALS model can be used to estimate the basic transport parameters k_i, k_{chem}, D_i, D_{chem}, and the thermodynamic factor. Consequently, we have investigated in detail the performance of a nanostructured electrode in a symmetric cell using ac impedance spectroscopy. Analyses of the results using the ALS model give new insights into the performance of nanostructured cathode materials. The data suggest that the thermodynamic factor, a measure of how easy it is to create oxygen vacancies, is much higher than observed in conventional cathodes. As a result, the electrode composition changes little with temperature and oxygen partial pressure, the large chemical contribution to the expansion is reduced, and the electrode has better stability. We also have shown that using nanoparticles does not significantly affect the fundamental material parameters (surface exchange and diffusion coefficients) and that the very low ASR for nanostructured LSCO (0.09 ohm cm^2 at 600 °C) is due to the PLD synthesis method that gives a very high surface area (80 μm^{-1}).

The present results and those of others demonstrate that nanostructured electrodes of very high surface area can have low cathode ASR values and thermal stability. This makes possible the use of such electrodes in the temperature range appropriate for micro-solid-oxide fuel cells and permits the use of materials with higher intrinsic activity which at higher temperatures would react with electrolytes.